IIETA International Information and Engineering Technology Association
Advancing the World of Information and Engineering

Revue des Composites et des Matériaux Avancés-
Journal of Composite and Advanced Materials
Vol. 33, No. 4, August, 2023, pp. 267-274
Journal homepage: http://iieta.org/journals/rcma

Modulating Magnetic Properties of Ferrite $Cu_{1-x}Mg_xFe_2O_4$ via RF Plasma Exposure: Effects of Magnesium Concentration

Alyaa Hefdhi Abbas Aziz[1*], Mohammed A. Al-Shareefi[1], Abdulhussain Abbas Khadyair[2]

[1] Department of Physics, College of Science, University of Babylon, Hillah 51002, Iraq
[2] Department of Physics, College of Education, University of Al-Qadisiyah, Ad Diwaniyah 58002, Iraq

Corresponding Author Email: sci.alyaa.hofdhy@uobabylon.edu.iq

https://doi.org/10.18280/rcma.330408

Received: 28 June 2023
Revised: 15 August 2023
Accepted: 21 August 2023
Available online: 31 August 2023

Keywords:
sol-gel, RF Plasma, magnetic properties, hysteresis loop, coercive force, X-ray diffraction

ABSTRACT

In this study, the magnetic compound $Cu_{1-x}Mg_xFe_2O_4$ is synthesized using the sol-gel method at distinct magnesium concentrations (x = 0, 0.2, 0.4, and 0.6) to investigate the influence of RF plasma exposure on its structural and magnetic properties. X-ray diffraction analysis, applied to examine the prepared ferrite, confirms the formation of the face-centered cubic (FCC) structure in the samples. Utilizing X-ray diffraction broadening and Scherrer's equation for particle size determination, sizes are found to range from 37.73 nm to 19.870 nm prior to plasma exposure and 30.35 nm to 19.115 nm subsequent to exposure. The study of the compound's magnetic properties demonstrates that the saturation magnetization spans from 33.5 to 32.1 emu/g, with an initial coercivity decrease from 150 to 50 Oe, further diminishing as magnesium concentration increases. Notably, following plasma exposure, alterations in saturation magnetization values (35.32–27.4 emu/g) and coercivity (150–25 Oe) are observed. The results underscore the impact of rising magnesium concentrations and plasma exposure on the compound's structural properties, potentially attributable to atomic rearrangement within the crystalline structure. In terms of magnetic properties, a reduction in coercive force following plasma exposure is discerned, thereby enhancing the ferrite's properties, which are applicable in transformer cores to minimize eddy currents.

1. INTRODUCTION

Spinel-organized nano-ferrites are as yet a significant subject of exploration in view of their wide applications in modern and mechanical fields [1]. Magnesium Ferrite, $MgFe_2O_4$, with its cubic structure, high electrical resistance, and high saturation magnetization value, belongs to an inverted spinel group. It finds applications in magnetic technology such as iron cores and transformers, gas sensors, microwaves [2]. The magnesium ferrite for high intensity contrasted with different ferrites when the grain volume is in the μm range [3]. The structure construction of spinel comprises two lattices of grid locales, destinations are tetrahedral (with four neighbours of oxygen atoms, they are known as A sites) and octahedral locales (with six neighbours of oxygen atoms, which are known as B sites) [4]. Because there are two kinds of crystal locations, the magnetic and electrical properties of spinel ferrite can be influenced by the locations of ions, and cation redistribution [5]. Copper ferrite has a spinel-type FCC chassis with a quadrangular shape that is only stable at room temp steady, which is caused by the Jahn-Teller distortion effect that occurs at room temperature. This leads to the formation of copper in a tetragonal shape [6]. There are two types of ferrites, one of which is soft and characterized by its low coercive force and high magnetization. They are used in microwave devices and inductors. Hard ferrite has a high coercive force and this leads to difficulty in removing magnetism. It is used in creating permanent magnetic devices such as those used in refrigerators, electric motors, and amplifiers [7].

Plasma, an ionized gas, is produced through the disintegration of polyatomic gas molecules or the expulsion of electrons from monatomic gas shells. Within this context, a state of macromolecular neutrality is a necessary condition for plasma [8]. Plasma treatment of the surface can be a high tensile surface coating resulting in bonding, coating, and printing when plasma and treated surfaces meet and create an object change and chemical reaction of auxiliary additives or produce a rough pattern or form a dense interlocking layer [9]. RF plasma is commonly used as a surface treatment or precipitation technology. Low-temperature plasma is used in a variety of industries, including electronics, and aerospace [10]. Radiofrequency plasma contains high-energy ions and widely reactive species that are used in surface etching and thin-film semiconductor deposition [11]. Magnetron sputtering differs from traditional vacuum discharge methods in that magnets are added behind the cathode to generate magnetic fields that focus the plasma in a narrow spot on the target, increasing the sputtering process [12]. Magnetron spray is currently widely used for depositing nanostructured films and thin films for superconducting materials [13]. Using the spontaneous combustion (sol-gel) technique, spinel ferrite (magnesium ferrite) was prepared and doped with a divalent element, copper, to synthesize the compound $Cu_{1-x}Mg_xFe_2O_4$. The compound was formed into circular discs with a diameter of 20 mm, then subjected to spray plasma to deposit a layer on

the discs' surface. This process was followed by an examination of the plasma's impact on the prepared samples. The aim was to form a protective layer on the prepared ferrite surface against corrosion, making it suitable for use in transformer cores. Kanagesan et al. [14] produced nanocrystalline magnesium ferrites ($MgFe_2O_4$) with an average grain size of about 20 nm, synthesized using the microemulsion technique. XRD analysis revealed that the synthesized samples possessed a single cubic spinel phase without any trace of impurity. The hysteresis loop exhibited ferromagnetic behaviour. Le Trong et al. elaborated on iron cobaltite thin films, $Co_{1.75}Fe_{1.25}O_4$, with a spinel structure, which were created by radio-frequency (RF) magnetron sputtering. They examined the influence of argon pressure on the structure, microstructure, and physical properties of the films. According to their study, XRD revealed the formation of spinel structure with space iron–cobalt oxide of one spinel phase. The increase in argon pressure also leads to the lowering of both saturation magnetization, and coercive field at 150 K [15]. Hammad et al. synthesized $Cu_{1-x}Mg_xFe_2O_4$ nanoferrites using a co-precipitation method. The crystallite size, determined from XRD results, showed that the lattice constant decreased from 8.465 Å to 8.334 Å. With increasing Mg concentration, the nanoparticle size decreased from 17.4 to 10.2 nm. With the increase of Mg^{+2} ion, saturation magnetization, and remanent magnetization decreases [16].

2. MATERIALS AND METHODS

2.1 Sample preparation

Copper powders with magnesium replacements $Cu_{1-x}Mg_xFe_2O_4$ (x=0, 0.2, 0.4, 0.6) were prepared by sol-gel spontaneous combustion process. The raw resources used are of analytical quality $Cu(NO_3)_2{\cdot}6H_2O$, $Mg(NO_3)_2{\cdot}9H_2O$, Fe(NO3)2·9H2O, $C_6H_8O_7$ (citric acid monohydrate) and NH4·H2O (ammonia), the materials whose values are shown in Table 1. To prepare test solutions, metal nitrate and citric acid were weighed on a sensitive scale and dissolved in deionized water. By adding ammonia, the pH of the metal nitrate solution was raised from 7 to 8. The assorted solutions were superheated in a temperature regulator water bath at 60°C, then gradually increased the temperature and stirred continuously for three hours to form a dry gel. The gels were dried for 2 hours at 120°C before being incinerated in spontaneous burning to produce a loose powder igniting them in room temperature air. Figure 1 illustrates two stages of the ferrite burning process: panel (a) shows the initial stage of burning, while panel (b) presents the final or advanced stage of the process.

The powder particles were ground and sintered in a thermal oven at 1100 degrees Celsius for a period of 6 hours, after which it is left inside the oven to cool for a period of 24 hours, after that we repeat the grinding process until it becomes homogeneous. Then the powder was mixed with 6% glycerin, before the powder was compressed by a hydraulic press with a pressure of 150 kN within two minutes, molds were used in the form of disc with a 20 mm diameter as shown in Figure 2.

The work will be done in two stages: before exposing it to the plasma, and then when the samples are placed in the RF Magnetron Sputtering. Figure 3 depicts a diagram of the components of the RF sputtering system utilized in this work, as the sputtering system is made up of three major components: the chamber, the RF power supply, and the vacuum system. As a working gas, pure argon gas (99.9% impurity) was used. The chamber covered by an upper surface with three magnetron targets built-in one of it is head material from copper connected to RF power supply of 200 W. The second part is the control box which contains a touch screen to control starting of system, flowing of gas, sample rotation speed (1440 rpm), maximum vacuum pressure (1.5*10-3 mbar), frequency (50 Hz), voltage (220 V), and stage temperature setting to reach to (523 K), in addition to inlet gas and air switch.

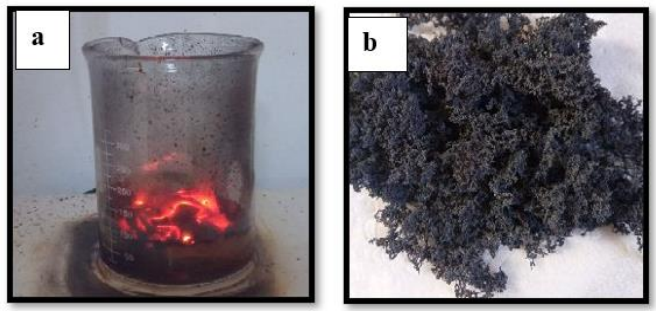

Figure 1. Burning ferrite

Figure 2. The sample disc (20 mm in diameter)

Table 1. The purity of the used raw materials

Chemical Formula	Molar Weight (g.mol-1)	Purity
$Cu(NO_3)_2.3H_2O$	241.60	95%
$Mg(NO_3)_2{\cdot}9H_2O$	256.41	99%
$Fe(NO_3)_2{\cdot}9H_2O$	404	98%
$C_6H_8O_7$	192.12	99%
NH_4	35.05	25%

In this work, models of ferrite were prepared using a sol-gel method have been deposited as follows: Clean the brass target, the clean substrate is placed on the sample stage in the centre of the chamber, close the chamber lid, rotary vacuum started, set the temperature up to 523 K. After reaching the pressure required, the device is turned on. The chamber must be filled with argon gas, RF source is turned on, reducing reflected power until it reaches zero for the most efficient plasma generation, at this point the deposit process starts, and the deposit time lasted 2 hours.

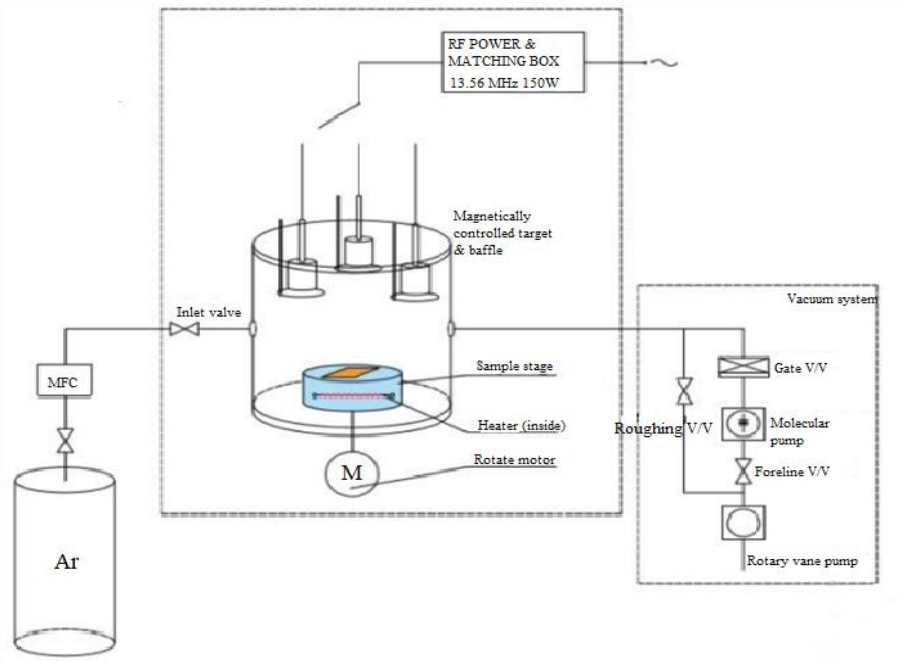

Figure 3. The schematic of RF magnetron sputtering setup

2.2 Sample characterization

An XRD device was used to examine the crystal structure of the samples and structural information of the prepared ferrite (X' Pert PW 3040/60) was verified. The radiation is found for target Cu-K α with wavelength (0.15405 nm) in Par-e-Tavous Research Institute- Mashad-IRAN.

The VSM device was used to measure the magnetic hysteresis loop of the sample to measure and assign magnetic properties to it such as coercive force, saturated magnetization, and remnant magnetization. The magnetic properties were measured at the Spadana Institute of Materials Science in Isfahan-Iran by using a device (Model 7400 VSM USA) where the applied field strength ranged between ± 15000 Oe at room temperature.

3. RESULTS AND DISCUSSION

3.1 Analysis of X-ray Diffraction (XRD)

Using an XRD device, the powdered $Cu_{1-x}Mg_xFe_2O_4$ samples were examined to determine the different phases and structural properties. The crystal structure and synthetic information of the prepared ferrite were verified (X' Pert PW 3040/60) diffractometer (λ=1.54). The X-ray diffraction diagram is useful for diagnosing the material by comparing the prepared material's outcomes to the International Centre of Diffraction Data (ICDD).

Figure 4(a-d) presents the XRD spectra of the compound $Cu_{1-x}Mg_xFe_2O_4$. Upon examination, as depicted in subfigures 4a and 4b, diffraction peaks are observed at the crystal planes (022), (222), (004), (224), (115), (044), and (226). These peaks confirm the presence of a face-centered cubic (FCC) spinel phase in all the prepared samples of $Cu_{1-x}Mg_xFe_2O_4$. These samples, doped with various ratios of Mg^{+2} concentrations, show no evidence of secondary phases.

The XRD patterns show the prepared sample's pure crystalline nature with no secondary phase impurities, confirming the product's high pureness of the cubic spinel construction. The prevalent pattern of crystallization development (222) the distance between the peak increases and decreases depending on the concentration Mg^{+2}, as well as that there is a slight shift to the right in the copper ferrite, which shows a reduction in the crystalline frit of copper. There was a little change in the locations of the diffraction peaks of both the host and the doped samples into higher diffraction angles. This indicates that Cu^{+2} ions were concurrently substituted with Mg^{+2} ions. These findings are consistent with the idea that the substituted ions are able to fill the positions of the crystallographic sites, this result is nearly close to obtained by Hammad et al. [16]. Before plasma exposure when the magnesium ion concentration increases lead to increasing pressure on the crystal structure it leads to a decrease in the crystallite size of the nanoscale, because when the magnesium ion is replaced by the copper ion, the particle size decreases because the ionic radius of the magnesium (0.75) A° is larger than the ionic radius of the copper ion (0.73) A° [16]. Table 2 reveals the structural components' parameters measurements.

After exposure to plasma, the prevailing trend of crystal growth remained at (222), and a peak at (111) appeared when x equalled 0 and 0.4, as shown in Figures 5(a) and 5(c). However, when x equalled 0.6, not only did the peaks at (111) and (113) appear, but the peak at (226) also disappeared, as demonstrated in Figure 5(b) and 5(d). Results such as these on the relative intensity of some reflective have been reported by a study and have been attributed to a distortion in the cubic lattice after plasma exposure, or because of rearranging the atoms in the crystal lattice and changing their locations. Through the shape of samples for x-ray measurements after exposure to plasma, much fewer peak intensities were found in the ones when the Mg ion concentration was increased. The maximum intensity peak before plasma exposure is (222), which is well suited to the same angle after plasma exposure.

The XRD study indicates that the sample that is not exposed to plasma and the sample that is expose to plasma are essentially cubic and it is known that these differences in XRD shapes are because the copper ferrite has undergone Jahn-Teller distortion, this result is nearly closed to obtained by Desai et al. [17].

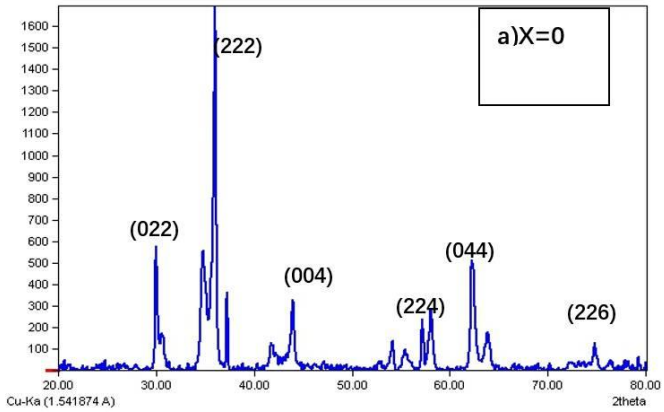

(a)

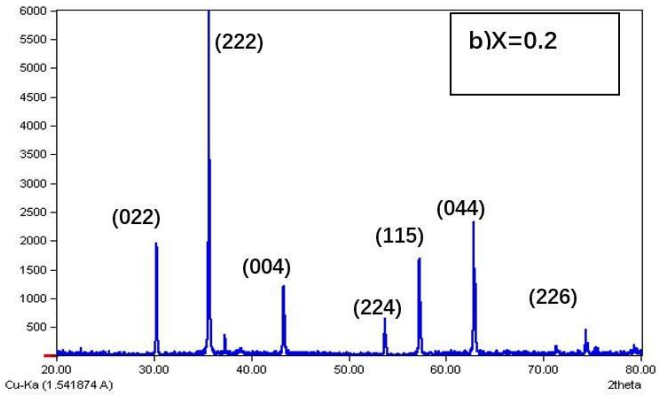

(b)

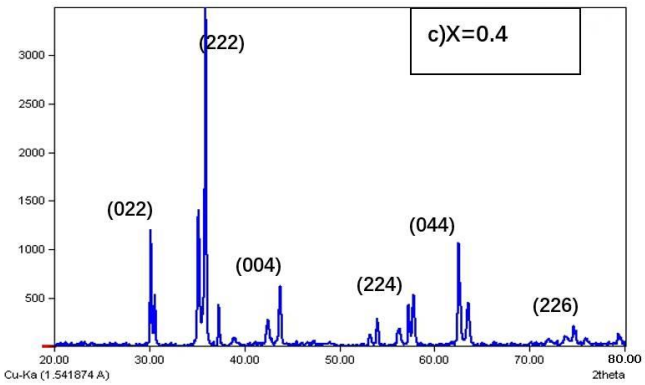

(c)

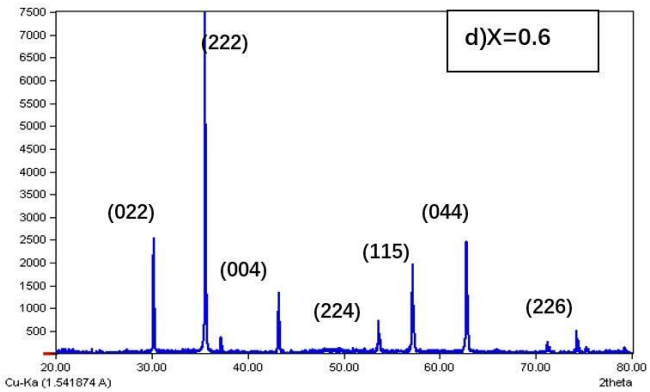

(d)

Figure 4. X-Ray patterns of $Cu_{1-x}Mg_xFe_2O_4$ with different ratio(x) Mg before plasma exposure

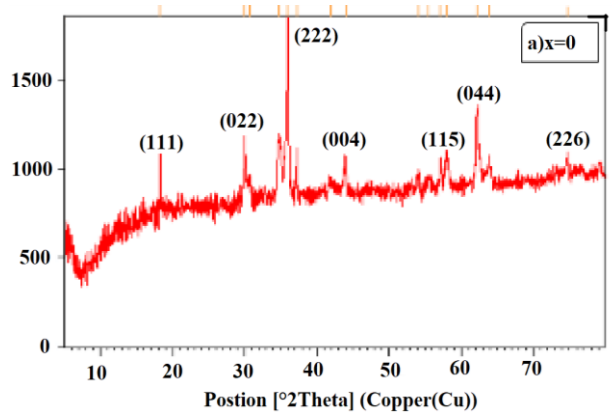

(a)

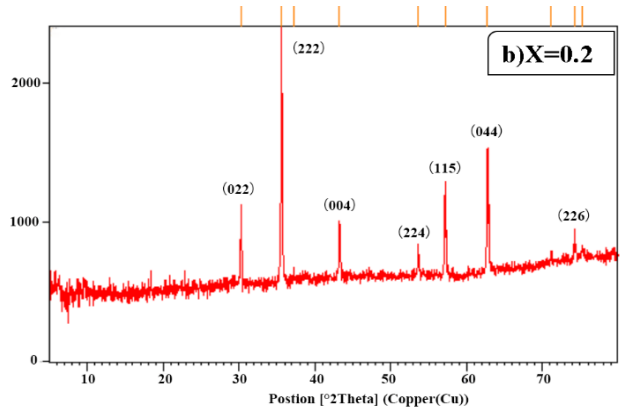

(b)

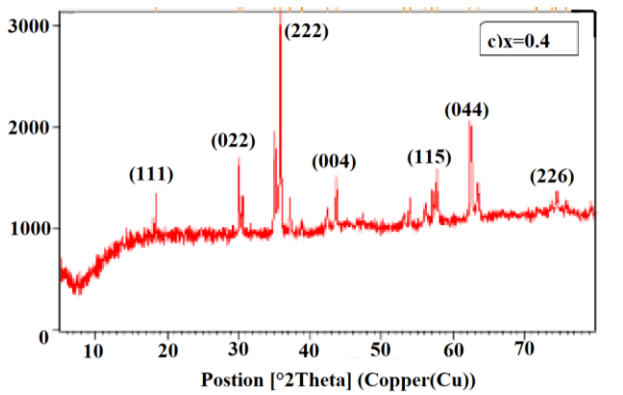

(c)

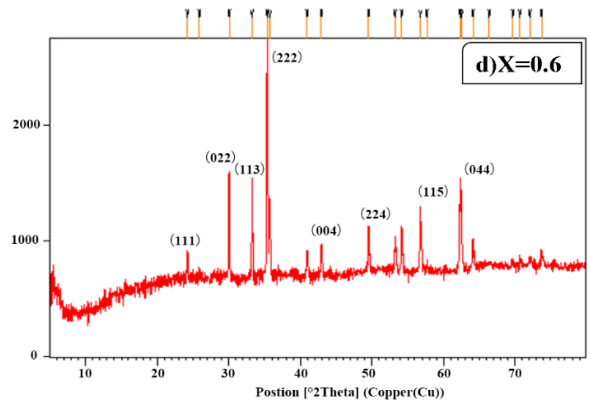

(d)

Figure 5. X-Ray patterns of $Cu_{1-x}Mg_xFe_2O_4$ with different ratio(x) Mg after plasma exposure

Table 2. Structural parameters of $Cu_{1-x}Mg_xFe_2O_4$. before plasma exposure

Component	(hkl)	Peak-Position (2theta)	FWHM	Size of Crystallite D (nm)	d_{hkl} (nm)	a(Å)
$CuFe_2O_4$	(222)	35.97	0.137	37.733	0.2494	8.6392
$Cu_{0.8}Mg_{0.2}Fe_2O_4$	(222)	35.68	0.157	25.642	0.2513	8.7050
$Cu_{0.6}Mg_{0.4}Fe_2O_4$	(222)	35.49	0.136	27.370	0.2511	8.6981
$Cu_{0.4}Mg_{0.6}Fe_2O_4$	(222)	35.59	0.157	19.870	0.2536	8.7847

Table 3. Structural parameters of $Cu_{1-x}Mg_xFe_2O_4$. after plasma exposure

Component	(hkl)	Peak-Position (2theta)	FWHM	Size of Crystallite D (nm)	d_{hkl} (nm)	a(Å)
$CuFe_2O_4$	(222)	35.97	0.137	30.35	0.2494	8.7676
$Cu_{0.8}Mg_{0.2}Fe_2O_4$	(222)	35.68	0.157	25.121	0.2513	8.7255
$Cu_{0.6}Mg_{0.4}Fe_2O_4$	(222)	35.49	0.136	25.470	0.2511	8.7431
$Cu_{0.4}Mg_{0.6}Fe_2O_4$	(222)	35.59	0.157	19.151	0.2536	8.7620

Table 3 shows structural parameters after plasma exposure. The Scherrer equation given under Eq. (1) is used to calculate the granular size [7]. In this equation, a constant (k) is also named the shape factor; β is the full-width half maxima; θ is Bragg's diffraction angle; and λ is the wavelength of the X-rays (1.545) nm.

$$D = k\lambda/(\beta\cos\theta) \quad (1)$$

3.2 Magnetic properties

The magnetic characteristics of a as samples as well as the magnetic field strength was measured with a resonance sample magnetometer (VSM). Figure 6(a-d) depicts the hysteresis loop analysis of $Cu_{1-x}Mg_xFe_2O_4$ ferrite at x = (0, 0.2, 0.4, 0.6), the narrow curves indicate the soft ferrite spinel behaviour, Figures 6(a-d) illustrate the magnetic behaviour of the samples prior to plasma exposure, clearly demonstrating distinct magnetic properties such as magnetic saturation (Ms), residual magnetization (Mr), and coercive field (Hc).

As the narrow hysterical loop indicates a loss of magnetism, and this is one of the properties of soft spinel, a substance that does not store magnetism, we can see that the area of the hysterical loop decreases with increases (x) for Mg^{+2} ion. Table 4 shows the saturation magnetization (MS), coercivity (Hc), rest (Mr) of the sample with Cu^{+2} before plasms exposure.

It is clear from the Table 4 that the replacement of magnesium with copper leads to fluctuation in the values of magnetization. Mg substitution enhances to a lesser extent than saturated magnetization values at x=0.2, which may be due to configuration Mg^{+2} ion in cubic structures.

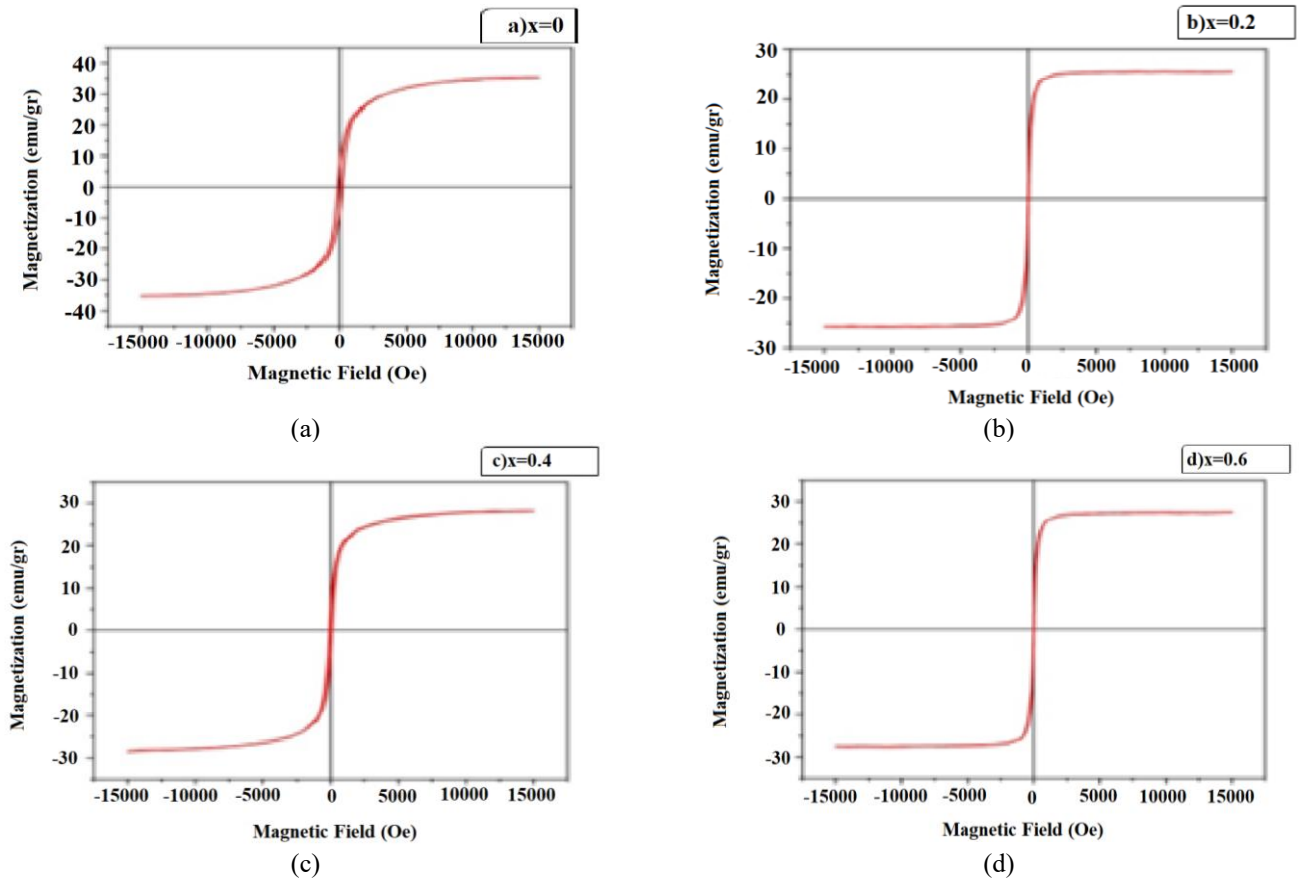

Figure 6. Magnetic hysteresis curves of $Cu_{1-x}Mg_xFe_2O_4$ with different ratios of Cu at sintering of 1100°C before plasma exposure

Table 4. Magnetic properties (Ms, Mr, Hc) versus manganese ratio, pre-plasma exposure

Ratio(x)	Component	Ms emu/g	Mr emu/g	Hc Oe
x=0	$CuFe_2O_4$	33.5	7.9	150
x=0.2	$Cu_{0.8}Mg_{0.2}Fe_2O_4$	26.15	2.22	35
x=0.4	$Cu_{0.6}Mg_{0.4}Fe_2O_4$	32.61	2.21	75
x=0.6	$Cu_{0.4}Mg_{0.6}Fe_2O_4$	32.1	2.7	50

Table 5. Post-plasma exposure magnetic properties (Ms, Mr, Hc) as a function of manganese ratio

Ratio(x)	Component	Ms emu/g	Mr emu/g	Hc Oe
x=0	$CuFe_2O_4$	35.32	7.84	150
x=0.2	$Cu_{0.8}Mg_{0.2}Fe_2O_4$	25.45	1.64	51
x=0.4	$Cu_{0.6}Mg_{0.4}Fe_2O_4$	28.2	4.35	50
x=0.6	$Cu_{0.4}Mg_{0.6}Fe_2O_4$	27.4	1.96	25

This is reflected in the coercive force, whose values varied with increasing and decreasing proportions of the Cu^{+2} ion. Table 4 illustrates a decrease in coercive force with increasing concentrations of Mg. This reduction in coercivity may be attributed to variations in crystal magnetism and changes in exchange properties, potentially resulting from spin disturbances on the particle surfaces [16]. Then the saturated magnetization increases as the magnesium ion concentration increases the reason for the increase in magnetic saturation is the rearrangement of the sites between the ions, as well as the magnetic behaviour of the Mg^{+2} ion, which is larger than the Cu^{+2} ion because the radius of the magnesium ion is greater than the radius of the copper ion [17]. Figure 7 depicts the hysteresis loop of the same ferrite compound after being exposed to plasma rays via a (RF) system and for the same ratios at x = (0, 0.2, 0.4, 0.6), from the shapes, it is clear that it corresponds to the natural behaviour in which all natural rings confirm the soft magnetism of Cu-Mg ferro. Magnetic properties of spinel ferrite are affected by various factors, including the path of synthesis, and the distribution of the cation on the tetrahedral and octahedral sites, and increasing crystalline size with (x). The magnetic properties of ferrite nanoparticles can be modified from using different doping ions [18].

The magnetic properties of spinel ferrite behaviour are indicated by the narrow curves. Figure 7 shows the loop magnetization or hysteresis curves of the analysed samples of the $Cu_{1-x}Mg_xFe_2O_4$ complex after exposure to plasma [19]. The ferrite hysteresis loop was plotted using the applied field and the corresponding magnetization. From the shapes, it is clear that it corresponds to the natural behaviour in which all natural rings confirm the soft magnetism of Cu-Mg ferro [20].

In Table 5 the magnetic parameters are calculated using the hysteresis loop. That it is evident from the table that exposure to plasma lead the decrease and increase in the saturation region of the ratio of (x) as unexposed samples the same goes for values Mr and Hc, an increase in Ms is observed in the plasma-treated and higher the value at 35.8 emu/g after replacement with $MgFe_2O_4$. This escalation in saturation magnetization correlates with direct contact of ferrite samples with microwave plasma, change in compulsion can be associated with surface effects generated during plasma exposure [21].

Thus, analysis of magnetic properties by microwave plasma treatment is an effective technique used to modify ferrite surface and can be valuable in newer applications. When the ferrite samples are exposed directly to the plasma, the mobility can be improved magnetic dipoles are significantly increased due to the higher temperature, thereby enhancing saturation magnetization [22].

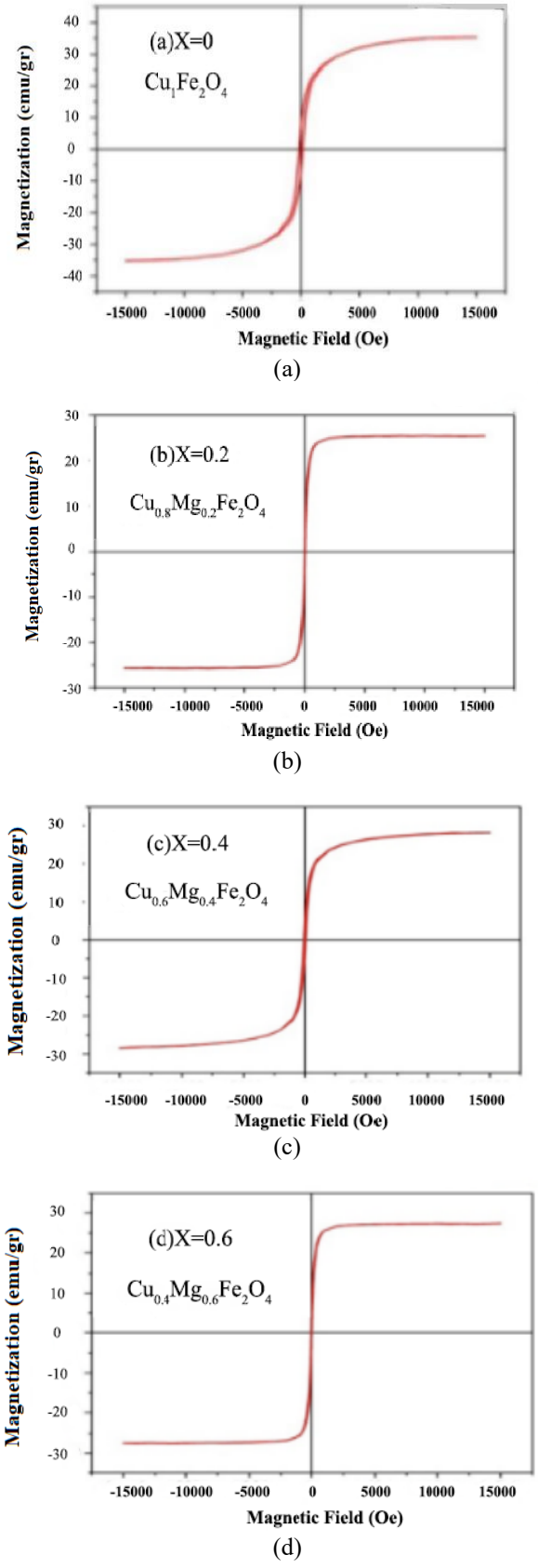

Figure 7. Magnetic hysteresis curves of $Cu_{1-x}Mg_xFe_2O_4$ with different ratios of Cu at sintering of 1100 ˚C after plasma exposure

4. CONCLUSIONS

The present study indicates that it is possible to the magnetic nanoparticles $Cu_{1-x}Mg_xFe_2O_4$ were prepared by the sol-gel combustion method, it has advantages due to the ease of purification of liquids (being the starting material for the process), high purity materials are produced in prepare ferrites materials and low cost, a single-phase spinel structure was demonstrated to form by the X-ray diffraction pattern of these composites.

The tests conducted showed to samples before exposing plasma a decrease in the crystal size of $Cu_{1-x}Mg_xFe_2O_4$ ferrite with increasing Mg concentration from (37.733) nm at (x=0) to (19.870) nm at (x=0.6), because Copper ions have a more condensed shape, hence their radius is less than that of magnesium ions and the lattice parameter obtained analysis shows increasing trend from 8.639Å to 8.784Å with the substitution of Cu–Mg ions in $Cu_{1-x}Mg_xFe_2O_4$. The samples are exposing to the same concentrations to plasma using the RF system using the ZnO target material to the ferrite compound, and new peaks (111) and (113) were formed after exposure to plasma. There was a discernible shrinkage in the size of the crystal from (30.35) nm to (19.115) nm and the lattice parameter from (8.76766) Å to (8.7620) Å, with an increase in magnesium concentration. Thus, X-ray measurements showed that samples exposure to plasma have a cubic spinel structure, and the variation of structural parameters with the exposure is irregular, because the plasma exposure has a strong tendency for molecular adsorbed on the surface of the material during the deposition process, which leads in restricted mobility of incoming particles and a tiny particle size as a consequence.

The hysteresis loop is show of $Cu_{1-x}Mg_xFe_2O_4$ ferrite at room temperature, the soft ferritic materials is use in this research have a small magnetic remaining loop, Where we notice a decrease in the area of the hysteretic ring with the increase of Mg^{+2}, The compound $Cu_{1-x}Mg_xFe_2O_4$ before exposure to plasma, we notice a continuous fluctuation in the saturated magnetization values (33.5-32.1)emu/g and the decrease in coercivity (150-50)Oe because of its particles size and the difference in crystal magnetism and the change in exchange properties due to the spin perturbation on the particle surface. After exposing the analysed samples of $Cu_{1-x}Mg_xFe_2O_4$ to plasma will form the curve of loop hysteresis. That exposure to plasma actually led to an increase of Ms (35.32-27.4) emu/g, this escalation in saturation magnetization is related to the direct contact of the ferrite samples with the microwave plasma. As well as the result of improving the movement of diodes magnetic poles of the material due to its high temperature after exposure to the plasma, which enhances the saturation magnet. The decrease in the force coercive (150-25) Oe for it indicates of soft ferrite and good they can be used as a core for electrical transformers and to eliminate eddy currents that cause most losses in electrical transformers.

For future work, it is possible of studying the compounds that were prepared in this work, after exposing it to plasma and depositing it on quartz as a thin film, and studying its electrical, optical and magnetic properties. Preparation of new compounds in formulas, as follows, $Cd_{1-x}Zn_xFe_2O_4$, $Mn_xZn_{1-x}Fe_2O_4$, $Mg_xZn_{1-x}Fe_2O_4$, $Mg_xCd_{1-x}Fe_2O_4$. Also, exposure to plasma, study and comparison of properties before and after exposure. It can Preparation of the same compounds with formulas $Mg_{1-x}Zn_xFe_2O_4$ where M are cations (Co, Ni, Mn, Cu) with changing PH using co-precipitation or sol-gel method.

REFERENCES

[1] Bharti, D.C., Mukherjee, K., Majumder, S.B. (2010). Wet chemical synthesis and gas sensing properties of magnesium zinc ferrite nano-particles. Materials Chemistry and Physics, 120(2-3): 509-517. https://doi.org/10.1016/j.matchemphys.2009.11.050

[2] Chen, Q., Rondinone, A.J., Chakoumakos, B.C., Zhang, Z.J. (1999). Synthesis of superparamagnetic $MgFe_2O_4$ nanoparticles by coprecipitation. Journal of Magnetism and Magnetic Materials, 194(1-3): 1-7. https://doi.org/10.1016/S0304-8853(98)00585-X

[3] Maehara, T., Konishi, K., Kamimori, T., Aono, H., Hirazawa, H., Naohara, T., Kawachi, K. (2005). Selection of ferrite powder for thermal coagulation therapy with alternating magnetic field. Journal of materials science, 40: 135-138. https://doi.org/10.1017/s10853-005-5698-x

[4] Dileep, K., Loukya, B., Pachauri, N., Gupta, A., Datta, R. (2014). Probing optical band gaps at the nanoscale in $NiFe_2O_4$ and $CoFe_2O_4$ epitaxial films by high resolution electron energy loss spectroscopy. Journal of Applied Physics, 116(10). https://doi.org/10.1063/1.4895059

[5] Solís, C., Somacescu, S., Palafox, E., Balaguer, M., Serra, J. M. (2014). Particular transport properties of $NiFe_2O_4$ thin films at high temperatures. The Journal of Physical Chemistry C, 118(42): 24266-24273. https://doi.org/10.1021/jp506938k

[6] Lakhani, V.K., Modi, K.B. (2010). Al^{3+}-modified elastic properties of copper ferrite. Solid State Sciences, 12(12): 2134-2143. https://doi.org/10.1016/j.solidstatesciences.2010.09.012

[7] Lokhande, C.D., Kulkarni, S.S., Mane, R.S., Han, S.H. (2007). Copper ferrite thin films: Single-step non-aqueous growth and properties. Journal of Crystal Growth, 303(2): 387-390. https://doi.org/10.1016/j.jcrysgro.2006.12.063

[8] Daltrini, A.M., Moshkalev, S.A., Swart, L., Verdonck, P.B. (2007). Plasma parameters obtained with planar probe and optical emission spectroscopy. Journal of Integrated Circuits and Systems, 2(2): 67-73. https://doi.org/10.29292/jics.v2i2.266

[9] Dyson, A., Bryant, P., Allen, J. E. (2000). Multiple harmonic compensation of Langmuir probes in RF discharges. Measurement Science and Technology, 11(5): 554. https://doi.org/10.1088/0957-0233/11/5/316

[10] Le Trong, H., Bui, T.M.A., Presmanes, L., Barnabé, A., Pasquet, I., Bonningue, C., Tailhades, P. (2015). Preparation of iron cobaltite thin films by RF magnetron sputtering. Thin Solid Films, 589: 292-297. https://doi.org/10.1016/j.tsf.2015.05.041

[11] Farheen, A., Singh, R. (2019). Effect of hydrothermal annealing on structure and magnetic properties of RF sputtered Mn-Zn Ferrite thin films. Materials Research Express, 6(11): 114001. https://doi.org/10.1088/2053-1591/ab45c2.

[12] Nawale, A.B., Kanhe, N.S., Patil, K.R., Bhoraskar, S. V., Mathe, V.L., Das, A.K. (2011). Magnetic properties of thermal plasma synthesized nanocrystalline nickel ferrite ($NiFe_2O_4$). Journal of Alloys and Compounds, 509(12): 4404-4413. https://doi.org/10.1016/j.matchemphys.2012.10.007

[13] Hasaani, A.S. (2016). Magnetic field effect on the characteristics of large-volume glow discharge in argon

at low pressure. Iraqi Journal of Science, 57(1A): 135-144.
[14] Kanagesan, S., Hashim, M., Tamilselvan, S., Alitheen, N.B., Ismail, I., Bahmanrokh, G. (2013). Cytotoxic effect of nanocrystalline $MgFe_2O_4$ particles for cancer cure. Journal of Nanomaterials, 2013: 165-165. https://doi.org/10.1155/2013/865024
[15] Le Trong, H., Bui, T.M.A., Presmanes, L., Barnabé, A., Pasquet, I., Bonningue, C., Tailhades, P. (2015). Preparation of iron cobaltite thin films by RF magnetron sputtering. Thin Solid Films, 589: 292-297. https://doi.org/10.1016/j.tsf.2015.05.041
[16] Hammad, T.M., Kuhn, S., Amsha, A.A., Hejazy, N.K., Hempelmann, R. (2020). Comprehensive study of the impact of Mg^{2+} doping on optical, structural, and magnetic properties of copper nanoferrites. Journal of Superconductivity and Novel Magnetism, 33: 3065-3075. https://doi.org/10.1007/s10948-020-05559-2
[17] Desai, M., Prasad, S., Venkataramani, N., Samajdar, I., Nigam, A.K., Krishnan, R. (2002). Annealing induced structural change in sputter deposited copper ferrite thin films and its impact on magnetic properties. Journal of Applied Physics, 91(4): 2220-2227. https://doi.org/10.1063/1.1433176
[18] Shirsath, S.E., Toksha, B.G., Jadhav, K.M. (2009). Structural and magnetic properties of In^{3+} substituted $NiFe_2O_4$. Materials Chemistry and Physics, 117(1): 163-168. https://doi.org/10.1016/j.matchemphys.2009.05.027
[19] Rudraswamy, B., Matteppanavar, S., Bharathi, P., Praveena, K. (2015). Magnetic properties of nanocrystalline $Mn_{1-x}Zn_xFe_2O_4$. In 2015 AIP Conference Proceedings, AIP Publishing, 1665(1). https://doi.org/10.1063/1.4917655
[20] Yasseen, F.A., AL-Shareefi, M.A.A. (2020). Preparation and study of the physical properties of the ferrite compound $Al_{1-x}Zn_xFe_2O_4$ using sol gel method. Journal of Xi'an University of Architecture and Technology, 12(3): 3363-3370.
[21] Safari, A., Gheisari, K., Farbod, M. (2022). The effect of plasma arc discharge process parameters on the properties of nanocrystalline (Ni, Fe) Fe_2O_4 ferrite: Structural, magnetic, and dielectric studies. Journal of Magnetism and Magnetic Materials, 541: 168536. https://doi.org/10.1016/j.jmmm.2021.168536
[22] Mohapatra, J., Xing, M., Elkins, J., Beatty, J., Liu, J. P. (2020). Size-dependent magnetic hardening in $CoFe_2O_4$ nanoparticles: Effects of surface spin canting. Journal of Physics D: Applied Physics, 53(50): 504004. https://doi.org/10.1088/1361-6463/abb622